MR-Compatible Ultrasound Through Transmission for Focused Ultrasound Thermal Therapy

Davi Cavinatto
Biomedical Engineering
University of Utah
Salt Lake City, UT, USA
davi.cavinatto@utah.edu

Taylor Webb
Radiology and Imaging Sciences
University of Utah
Salt Lake City, UT, USA
taylor.webb@utah.edu

Sarang Joshi
Biomedical Engineering
University of Utah
Salt Lake City, UT, USA
sarang.joshi@utah.edu

Douglas Christensen
Biomedical and Electrical and Computer Engineering
University of Utah
Salt Lake City, UT, USA
christen@ee.utah.edu

Allison Payne
Radiology and Imaging Sciences
University of Utah
Salt Lake City, UT, USA
allison.payne@hsc.utah.edu

2025 IEEE International Ultrasonics Symposium (IUS) | 979-8-3315-2332-9/25/$31.00 ©2025 IEEE | DOI: 10.1109/IUS62464.2025.11201505

***Abstract*—Focused ultrasound (FUS) therapies for cancer provide non-invasive precise thermal treatment to tissues. Current FUS treatment systems rely on magnetic resonance imaging (MRI), B-mode ultrasound imaging, or harmonic motion imaging for guidance. MRI has the advantage of quantitatively measuring temperature but the high cost and limited availability of MRI limit ultimate impact. An MR-compatible Ultrasound Through Transmission (UTT) system that can quantitatively assess tissue changes caused by temperature is being investigated as a replacement for the current standard of guidance. Two FUS 256-element transducers are mounted in a container with a sample placed at their coinciding geometric center. A FUS transmitter system is connected to the transmitter transducer, while a FUS research system samples the signal at the receiver transducer. A UTT protocol of 256 sequential single-element transmissions with reception on 256 elements is performed on three different samples: homogeneous gelatin phantoms, gelatin phantoms with attenuative inclusions, and porcine meat samples before and after thermal ablation. Hybrid Angular Spectrum (HAS) acoustic simulations are performed on the unheated gelatin samples segmented into regions with measured properties. Simulations are also done on the heated porcine sample segmented into regions with ablative temperatures based on MR temperature imaging. Measured UTT datasets are compared to HAS-predicted transmission data. Complex regression shows good agreement between the UTT-measured and HAS-predicted datasets. On homogeneous samples, the average complex correlation coefficient across all receiver elements is 0.8897. In 1 cm and 2 cm diameter inclusion samples, the correlation is 0.7994 and 0.6934, respectively. On the porcine meat sample, the pre-ablation average correlation is 0.6636, with a post-ablation average correlation of 0.6595. The data indicate that ablation of the tissue causes measurable changes in the received signal, but our simplified model is inadequate to capture the true tissue changes. Future work is investigating this discrepancy with more advanced modeling. The ultimate goal is to use physics-informed neural networks to predict tissue changes from the UTT received signal.**

***Index Terms*—Focused Ultrasound, Ultrasound Through Transmission, HIFU, Thermal Ablation, Tissue Characterization, Hybrid Angular Spectrum, Acoustic Simulation**

We acknowledge indirect support from Huntsman Cancer Institute's Cancer Center Support Grant.

I. Introduction

Ultrasound (US) has evolved from a purely diagnostic tool in oncology to a modality with significant therapeutic applications. Among these, High-Intensity Focused Ultrasound (HIFU) has emerged as a promising technique, enabling precise and non-invasive ablation of malignant tissue. Promising results have been reported for its use in treating prostate, liver, breast, pancreas, and bone cancers [1]–[5]. The effectiveness of these techniques critically depends on the quality of the guidance used in each procedure. Currently, magnetic resonance temperature imaging (MRTI) [6], B-mode ultrasound [7], and harmonic motion imaging (HMI) [8] are among the leading methods proposed for treatment guidance. Nonetheless, limitations of each imaging technique, such as insufficient contrast and resolution (B-mode US), only tissue stiffness assessment (HMI), and expense and limited accessibility (MRTI), have hindered the widespread adoption of HIFU treatments. Ultrasound-based modalities are still of particular interest due to their real-time imaging capabilities, cost-efficiency, and broad accessibility [9]. The integration of ultrasound guidance techniques into HIFU workflows has the potential to facilitate the broader clinical adoption and efficacy of focused ultrasound interventions in oncologic applications. Ultrasound Through Transmission, presented here, is one potential US candidate for HIFU guidance.

Ultrasound Through Transmission (UTT), similar to ultrasound tomography, employs a paired transmitter and receiver transducer to generate an image of tissue along the acoustic beam path. In HIFU applications, the acquired image represents the acoustic properties of the tissue, which undergo dynamic alterations during the ablation process. Despite having the potential to combine the same image quality levels of MRI guidance with the portability and availability of ultrasound, a system of this kind has not yet been used or validated

for HIFU use. The challenge lies in the validation of UTT with the gold standard of MRTI guidance, since the current technology is not MR-safe and has insufficient temporal resolution for real-time treatment monitoring [10] [11]. For this purpose, we have designed an MR-safe UTT device with receive/transmit transducer arrays that allow for concomitant HIFU treatment and partial aperture US tomography under a controlled MRTI environment. Following the capture of experimental data, computational acoustic models of the setup are created and simulated using Hybrid Angular Spectrum (HAS) and compared for accuracy.

In this study, three types of gelatin-based tissue-mimicking phantoms are used as samples for the validation of the accuracy of the UTT system: (A) homogeneous attenuating type, (B) homogeneous with cylindrical attenuating inclusions of different diameters, and (C) porcine meat. Since the receiver data are spatially-limited representations of the resulting transmission, the gradual increase in the level of spatial complexity between each sample tests the agreement between the acoustic forward model simulation and the measured partial tomography data in a clinical environment. These comparisons form the base for the derivation of tissue property changes from the received small-aperture UTT data, which, combined with physics-informed neural operator learning, can quantitatively detect tissue property changes caused by therapeutic ultrasound therapies.

II. Methods

A. UTT Hardware Setup

The imaging setup is comprised of two spherical 256-elements 1 MHz transducers [IMASONIC, France] mounted in a water-tight rectangular acrylic box. They are mounted on opposite sides of the box and face each other, with their geometric centers (100 mm) coinciding right at the center point of the box. A 3D-printed cradle, made of PLA, is placed at the center of the box, fastening a cylindrical sample holder. The PVC sample holder is loaded with a sample and sealed with ultrasound-transparent membranes glued to both sides (Fig. 1).

The transmitter transducer is driven by a HIFU generator and matching network system. The transmission protocol is created and controlled by Thermoguide [Image Guided Therapy, France]. The receiver transducer is connected to a Verasonics Vantage NXT system, which saves the experimental raw ultrasound wave data as MATLAB binary data. The raw data are processed by a MATLAB script, which uses FFT to find the amplitude and phase of the steady-state window of the received wave.

B. Experimental Protocol

Three types of samples are created: (A) homogeneous gelatin phantoms with five attenuation levels [12], (B) gelatin phantoms with attenuative inclusions of 1 and 2 cm diameter, and (C) porcine loin cuts (Fig. 2). Samples type A and B have their acoustic properties measured by a single-element UTT setup. Samples type C are characterized before and after ablation procedures using this paper's 256-elements UTT setup for speed of sound, and an acoustic radiation force balance setup for average attenuation. Average density is also measured for each phantom. See Table 1 for attenuation and speed of sound in each phantom. Before each UTT scan, samples are submerged in degassed, deionized water and fastened to the sample holder. All samples and water are kept at room temperature until the start of the experiment.

After loading the sample in the imaging setup, the UTT protocol is executed. In a serial manner, 256 transmitter elements are excited, each for 50 μs, accompanied by simultaneous recording using all 256 elements receiver channels. The 256 recordings, triggered by the 256 single-element transmission events, are recorded as a 1027x256x256 matrix, representing a raw US dataset of 256x256 transmission/reception pairs for a duration of 64.2 μs each. (Fig. 3)

For each experimental procedure, samples types A and B undergo one UTT protocol, repeated three times. Samples type C, due to their dual nature (pre- and post-ablation), undergo a pre- and post-ablation UTT protocol, each repeated three times. Guided by MRTI, phantoms type C undergo ablation

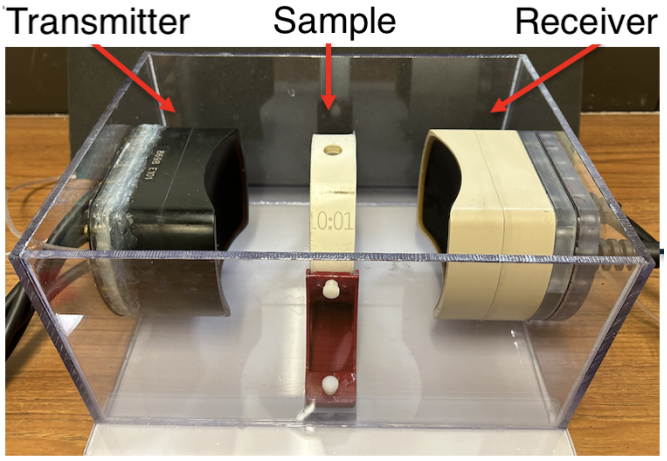

Fig. 1. The Ultrasound Through Transmission (UTT) Setup

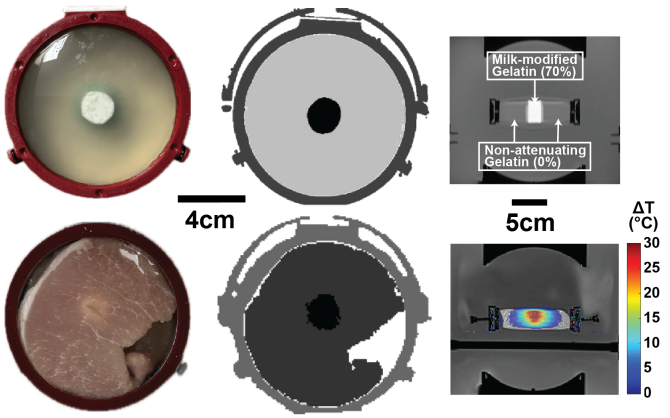

Fig. 2. Pictures of phantoms types B (top row) and C (bottom row), along with their corresponding acoustic simulation models and MRI/MRTI scans

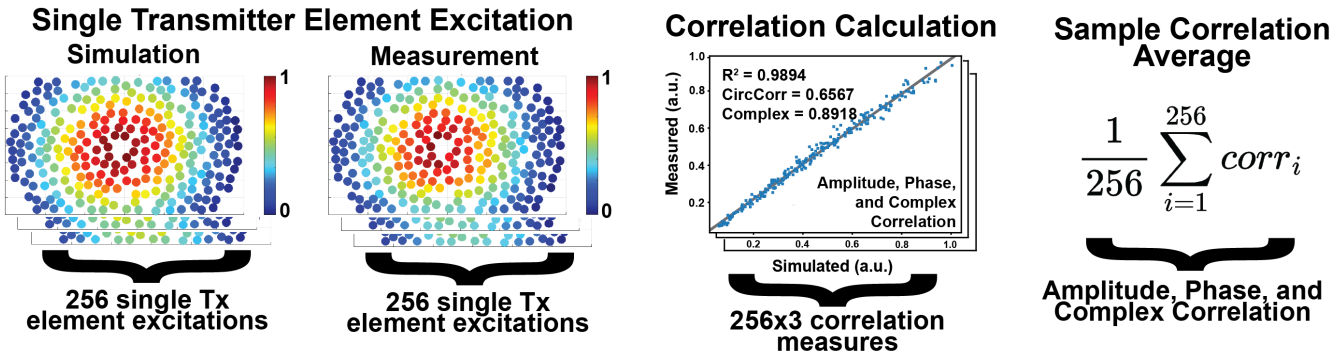

Fig. 3. Data acquisition and processing with an example of simulated and measured single transmitter reception, both normalized. Simulated and measured datasets are compared, generating 3 different correlation calculations for each experiment. Correlation metrics from the 256 experiments are averaged, generating three final correlation coefficients.

focused at the geometric center of the transducers until a temperature change of more than +35°C at the region of interest is achieved.

C. Simulation Protocol

A Hybrid Angular Spectrum (HAS) acoustic simulation model [13] is created based on (a) MRI data of the experimental setup and (b) the measured acoustic parameters of the samples. HAS, being an adaptation of the angular spectrum method for heterogeneous media, allows for the generation of complex pressure fields that spatially match our experimental design. The simulated complex pressure field, generated using a model of the experimental setup, allows the integration of the pressure at each receiver element. This enables an element-by-element direct comparison with the experimental measurements. For experiments with samples type A and B, the geometry of the simulation model is created using an MRI 3D VIBE scan of the experimental setup and Seg3D [University of Utah, USA], a segmentation software. For ablation experiments (samples type C), the model segmentation is aided also by MRTI images of the ablation procedure, which allow for the sectioning of regions exceeding a specific temperature threshold. In this paper, all post-ablation model segmentations use a 45°C temperature threshold (+20°C change from baseline).

TABLE I
MEASURED ACOUSTIC PROPERTIES FOR ALL SAMPLES

Sample	Atten. (Np/cm)	SoS (m/s)	Sample	Atten. (Np/cm)	SoS (m/s)
Homog. 10%	0.019	1530	PrePorkA	0.079	1602
Homog. 25%	0.033	1537	PostPorkA	0.091	1602
Homog. 40%	0.050	1549	PrePorkB	0.073	1582
Homog. 55%	0.056	1559	PostPorkB	0.085	1606
Homog. 70%	0.063	1570	PrePorkC	0.13	1600
Homog. 0%	0.0173	1526	PostPorkC	0.16	1627
Inclusion 70%	0.057	1568			

Color Code
Light gray - homogeneous gelatin type (samples type A).
Medium gray - gelatin with attenuative inclusion (samples type B).
Dark gray - porcine loin cuts (samples type C).

D. Data Analysis

After gathering the measured and simulated complex pressure datasets for each experiment, correlative analysis is performed. This is done through a complex scale invariant correlation function that outputs a numeric coefficient, which is equal to one when one of the complex-valued arrays are simply a scaled version of the other and zero when the arrays are orthogonal to each other [14]. Since each dataset contains 256 arrays of single-element experiment transmission events each simultaneously recorded by 256 receiver elements, this complex correlation is calculated 256 times (for each transmission event) and averaged across all events. This metric is a measure of the overall quality of the correlation between measured and simulated experiments.

Correlation measures using a standard linear regression model for amplitude analysis and a circular correlation for phase analysis are also reported. The linear correlation coefficient is the coefficient of determination (R^2) with bounds [0,1]. The circular correlation coefficient is bound to [-1,1], with its derivation described in detail elsewhere [15] [16]. In all measures, a 0 (zero) means low correlation and a 1 (one) means high correlation, with the circular analysis having also the possibility of inverse correlation represented by a -1 (minus one). The appropriate Fisher transformations were calculated prior to averaging and standard deviation calculations.

III. RESULTS

Complex correlation results show good agreement between UTT-measured and HAS-predicted data across all samples (Table 2). All homogeneous samples yielded very similar results and had their correlation coefficients averaged together.

Across all homogeneous samples, the standard deviations of the coefficient of determination (R^2), circular correlation coefficient, and complex correlations were 0.0017, 0.018,

TABLE II
CORRELATION BETWEEN SIMULATION AND MEASUREMENTS

Sample	R^2 (Ampl.)	Circ. Corr.	Complex Corr.
Homogeneous (avg.)	0.9500	0.5952	0.8897
Inclusion (1cm)	0.8815	0.4830	0.7994
Inclusion (2cm)	0.7219	0.4645	0.6934
Pre-ablation (Sample 1)	0.8627	0.3442	0.7181
Pre-ablation (Sample 2)	0.8883	0.3841	0.7168
Pre-ablation (Sample 3)	0.8365	0.2192	0.5558
Post-ablation (Sample 1)	0.7803	0.3037	0.7012
Post-ablation (Sample 2)	0.8062	0.3740	0.7636
Post-ablation (Sample 3)	0.7341	0.1638	0.5136
Color Code Light gray - homogeneous gelatin type (type A). Medium gray - gelatin with attenuative inclusion (type B). Dark gray - porcine loin cuts (type C).			

and 0.0092, respectively. On inclusion phantoms, the same standard deviations were 0.080, 0.013, and 0.053. On pre-ablation porcine phantoms the same standard deviations were 0.021, 0.085, and 0.076. On post-ablation porcine phantoms, the same standard deviations were 0.030, 0.11, and 0.11.

IV. DISCUSSION

In this paper, we report multiple correlation measures in acoustic phantoms using an MR-compatible Ultrasound Through Transmission (UTT) system, demonstrating that the Hybrid Angular Spectrum (HAS) acoustic modeling of different phantom types correlates well with measured UTT data. We show that the UTT system yields a high correlation coefficient for nearly all phantoms tested, despite their varied range in acoustic parameters and geometric complexities. Although the correlation drops off as the complexity of the model increases, the UTT system maintains sustains a minimum complex correlation of 0.5136, which indicates its potential as a data source for a physics informed neural network-based FUS guidance system. Further analysis of the correlation data revealed lower correlation in the simulated phase, which is a potential result of imperfections in the segmentation of the model and in the characterization of its acoustic properties. The latter issue was even more pronounced on samples type C, especially after ablation, as the method chosen for measurement of tissue attenuation is only able to obtain an average attenuation over the probed area. Additionally, the binary temperature thresholding method for segmentation of the MRTI data limited the quality of the acoustic model generated for ablated tissue, as attenuation and speed of sound likely follows a gradual continuous change in the focal region instead.

The limited number of sample complexities in this case report (3 types total), restrained the statistical significance of these findings across the entire spectrum of possible tissue shapes. Manual model segmentation and water temperature variability were also restrictions that likely lowered the correlation coefficients, especially in the ablation models. Future research will expand on the sensitivity analysis of the forward acoustic model correlation to the measured data, specifically defining the relation between increased degrees of model discretization and their effect in the correlation.

REFERENCES

[1] T. A. Jones, J. Chin, D. Mcleod, J. Barkin, A. Pantuck, and L. S. Marks, "High Intensity Focused Ultrasound for Radiorecurrent Prostate Cancer: A North American Clinical Trial," The Journal of Urology, Jan. 2018, doi: 10.1016/j.juro.2017.06.078.

[2] T. Yang et al., "HIFU for the treatment of difficult colorectal liver metastases with unsuitable indications for resection and radiofrequency ablation: a phase I clinical trial," Surg Endosc, vol. 35, no. 5, pp. 2306–2315, May 2021, doi: 10.1007/s00464-020-07644-y.

[3] D. Zulkifli, H. A. Manan, N. Yahya, and H. A. Hamid, "The Applications of High-Intensity Focused Ultrasound (HIFU) Ablative Therapy in the Treatment of Primary Breast Cancer: A Systematic Review," Diagnostics, vol. 13, no. 15, p. 2595, Jan. 2023, doi: 10.3390/diagnostics13152595.

[4] M. P. Fergadi et al., "A meta-analysis evaluating the role of high-intensity focused ultrasound (HIFU) as a fourth treatment modality for patients with locally advanced pancreatic cancer," Abdom Radiol, vol. 47, no. 1, pp. 254–264, Jan. 2022, doi: 10.1007/s00261-021-03334-y.

[5] A. Bongiovanni et al., "3-T magnetic resonance–guided high-intensity focused ultrasound (3T-MR-HIFU) for the treatment of pain from bone metastases of solid tumors," Support Care Cancer, vol. 30, no. 7, pp. 5737–5745, Jul. 2022, doi: 10.1007/s00520-022-06990-y.

[6] J. Blackwell et al., "Proton Resonance Frequency Shift Thermometry: A Review of Modern Clinical Practices," Journal of Magnetic Resonance Imaging, vol. 55, no. 2, pp. 389–403, 2022, doi: 10.1002/jmri.27446.

[7] E. Taka, G. Garay, W. Pereira, and G. Cortela, "Tracking of Thermal Ablation Using US B-Mode and Elastography," in 2024 IEEE UFFC Latin America Ultrasonics Symposium (LAUS), May 2024, pp. 1–4. doi: 10.1109/LAUS60931.2024.10553103.

[8] Y. Ran, J. Xu, X. Shi, Y. Liu, D. Cai, and X. Zhou, "Study on Preoperative HIFU Focus prediction Using Harmonic Motion Imaging," in 2024 IEEE Ultrasonics, Ferroelectrics, and Frequency Control Joint Symposium (UFFC-JS), Sep. 2024, pp. 1–4. doi: 10.1109/UFFC-JS60046.2024.10793613.

[9] E. S. Ebbini and G. Ter Haar, "Ultrasound-guided therapeutic focused ultrasound: Current status and future directions," International Journal of Hyperthermia, vol. 31, no. 2, pp. 77–89, Feb. 2015, doi: 10.3109/02656736.2014.995238.

[10] P. J. Littrup et al., "Multicenter Study of Whole Breast Stiffness Imaging by Ultrasound Tomography (SoftVue) for Characterization of Breast Tissues and Masses," J Clin Med, vol. 10, no. 23, p. 5528, Nov. 2021, doi: 10.3390/jcm10235528.

[11] J. Wiskin and J. Klock, "3D Ultrasound tomography timing validation for clinical deployment," in 2022 IEEE International Ultrasonics Symposium (IUS), Oct. 2022, pp. 1–3. doi: 10.1109/IUS54386.2022.9957317.

[12] A. I. Farrer et al., "Characterization and evaluation of tissue-mimicking gelatin phantoms for use with MRgFUS," J Ther Ultrasound, vol. 3, p. 9, Jun. 2015, doi: 10.1186/s40349-015-0030-y.

[13] U. Vyas and D. A. Christensen, "Extension of the angular spectrum method to calculate pressure from a spherically curved acoustic source," J. Acoust. Soc. Am., vol. 130, no. 5, pp. 2687–2693, Nov. 2011, doi: 10.1121/1.3621717.

[14] L. R. Rabiner and B. Gold, Theory and Application of Digital Signal Processing. Prentice-Hall, 1975, pp. 401.

[15] S. R. Jammalamadaka, A. Sengupta, and A. Sengupta, Topics in Circular Statistics. World Scientific, 2001, pp. 176.

[16] P. Berens, "CircStat: A MATLAB Toolbox for Circular Statistics," Journal of Statistical Software, vol. 31, pp. 1–21, Sep. 2009, doi: 10.18637/jss.v031.i10.